Dyes and Pigments 91 (2011) 145–152

Contents lists available at ScienceDirect

Dyes and Pigments

journal homepage: www.elsevier.com/locate/dyepig

Comparison of performance between benzoindoline and indoline dyes in zinc oxide dye-sensitized solar cell

Masaki Matsui [a,*], Masaya Kotani [a], Yasuhiro Kubota [a], Kazumasa Funabiki [a], Jiye Jin [b], Tsukasa Yoshida [c], Shinji Higashijima [a,d], Hidetoshi Miura [d]

[a] Department of Materials Science and Technology, Faculty of Engineering, Gifu University, 1-1 Yanagido, Gifu 501-1193, Japan
[b] Department of Chemistry, Faculty of Science, Shinshu University, 3-1-1 Asahi, Matsumoto, Nagano 390-8621, Japan
[c] Environmental and Renewable Energy System Division, Graduate School of Engineering, Gifu University, Yanagido, Gifu 501-1193, Japan
[d] Chemicrea Co., Ltd., 2-1-6 Sengen, Tsukuba, Ibaragi 305-0047, Japan

ARTICLE INFO

Article history:
Received 15 November 2010
Accepted 20 February 2011
Available online 16 March 2011

Keywords:
Dye-sensitized solar cell
Indoline dyes
Sensitizers
DFT calculations
Oxidation potential
Zinc oxide

ABSTRACT

The cell performance of novel benzoindoline dyes on zinc oxide prepared by template cathode electrodeposition method was compared with that of known indoline dyes. Among cyanoacrylic, single and double rhodanine acetic acid derivatives, the cyanoacrylic benzoindoline dye showed better performance than the indoline dye (D131) due to larger J_{sc} value which comes from its positive E_{ox} level and bathochromic UV–vis absorption band.

1. Introduction

Much attention has been paid to survey of sensitizers for dye-sensitized solar cell. Arylamine [1,2], dimethylfluorene [3], carbazole [4], and indoline dyes [5–9] have been reported as highly efficient organic sensitizers. Among these organic sensitizers, a double rhodanine indoline dye named D149 has been reported to show the excellent solar-to-electricity conversion efficiency (η) of 9.0% on titanium oxide [10]. More recently, D205, the *N*-octyl derivative of D149 on double rhodanine moiety, has been reported to show larger efficiency of 9.4% [11]. The structure modification [12,13], theoretical calculations [14], and decomposition mechanism [15] of indoline dyes have been also reported. Indoline dyes are used not only on titanium oxide [16–19] but also on zinc oxide [20,21]. The use of indoline dyes in solid-state [22,23], plastic film [24], and multi dye system solar cell [25] have been reported. Three kinds of indoline dyes having cyanoacrylic acid (D131), single (D102) and double rhodanine acetic acid (D149) moieties showing yellow, red, and purple hue, respectively, are known. Thus, indoline dyes are important compounds in dye-sensitized solar cell. When sensitizers absorb more photons, short-circuit photocurrent density (J_{sc}) increases. Therefore, survey of bathochromic sensitizers is of significance. Indoline dyes consist of intramolecular charge-transfer chromophoric system. When more electron rich benzoindoline ring is substituted with indoline ring, bathochromic shift in the UV–vis absorption band is anticipated. The zinc oxide cell performance of novel benzoindoline dyes was compared with that of known indoline dyes in this report.

2. Results and discussion

2.1. Synthesis

Benzoindoline dyes **11**, **12**, and **13** were synthesized as shown in Scheme 1. 1-Naphthylhydrazine (**1**) was allowed to react with 2-cyclopentane (**2**) to give benzoindole (**3**) followed by hydrogenation to afford benzoindoline **4**. This compound was allowed to react with an aryl bromide **5** to produce **6**, followed by formylation to give **7**. Compound **7** was allowed to react with cyanoacrylic acid (**8**), single and double rhodanine acetic acids **9** and **10** to afford **11**, **12**, and **13**, respectively. Known indoline dyes D102, D131, and D149 were also prepared in the similar way.

* Corresponding author. Tel.: +81 0 58 293 2601; fax: +81 0 58 293 2794.
E-mail address: matsuim@gifu-u.ac.jp (M. Matsui).

0143-7208/$ – see front matter © 2011 Elsevier Ltd. All rights reserved.
doi:10.1016/j.dyepig.2011.02.009

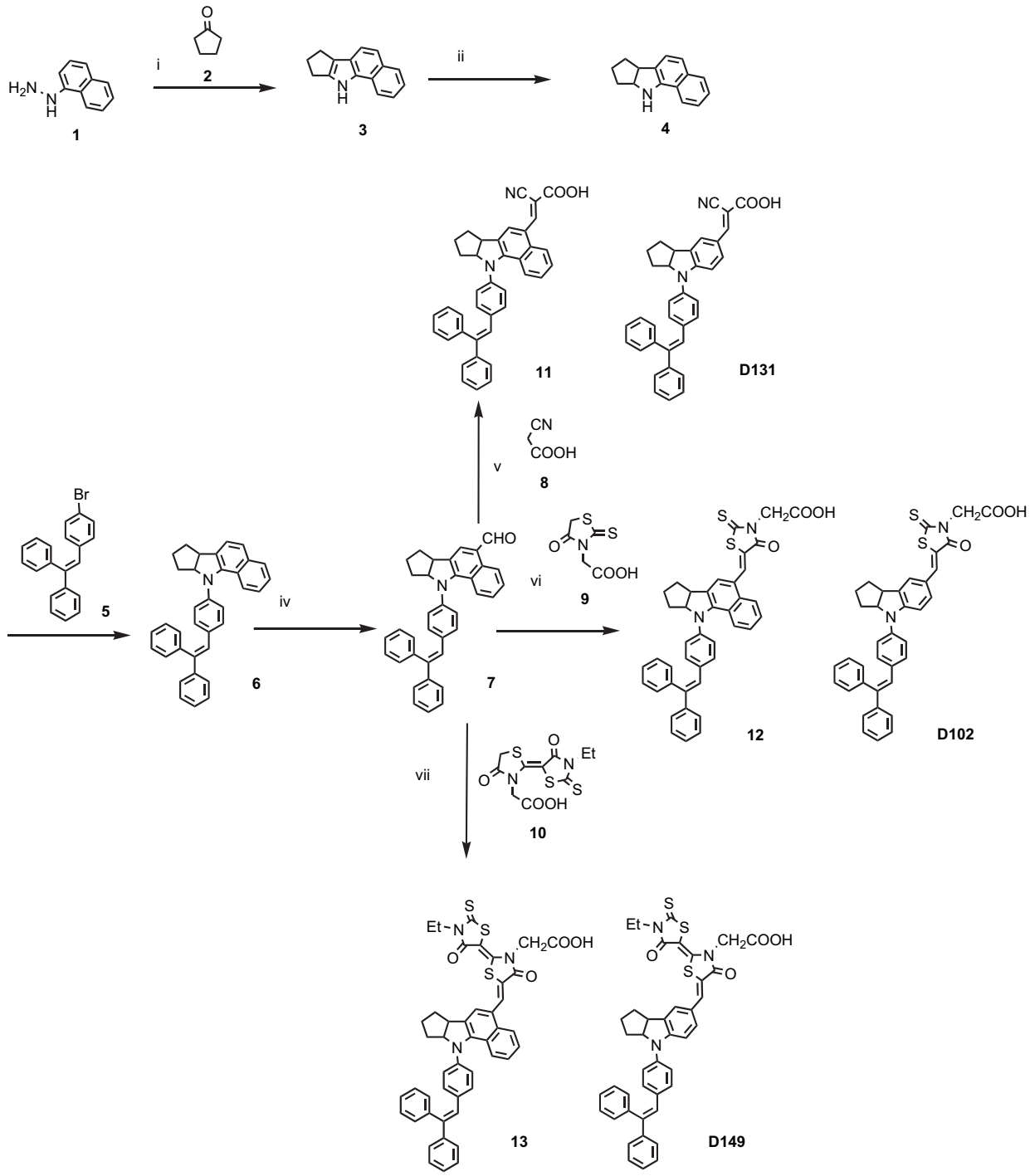

Scheme 1. i) AcONa, 2 (1.0 eq), AcOH, reflux, 2 h, ii) $NaBH_4$ (0.25 eq), AcOH, rt, 24 h, iii) 5 (1.0 eq), *t*-BuOK (1.2 eq), $Pd(OAc)_2$, $(t\text{-}Bu)_3P$, Xylene, 120 °C, 16 h, iv) DMF, $POCl_3$ (2.3 eq), 20 °C, 2 h, v) 8 (2.7 eq), piperidine (1.3 eq), MeCN, 120 °C, vi) 9 (1.0 eq), AcOH, $AcONH_4$ (0.4 eq), 120 °C, 90 min, vii) 10 (1.0 eq), AcOH, $AcONH_4$ (0.4 eq), 120 °C, 90 min.

2.2. UV–vis absorption and fluorescence spectra

The UV–vis absorption and fluorescence spectra of benzoindoline and indoline dyes in chloroform are depicted in Fig. 1. The results are also listed in Table 1. The first absorption maxima (λ_{max}) of benzoindoline dyes **11**, **12**, and **13** were observed at 507, 551, and 578 nm, respectively, there being *ca.* 40 nm more bathochromic than the corresponding indoline dyes D131, D102, and D149. The molar absorption coefficients (ϵ) of **11** (40100), **12** (39000), and **13** (50800) were smaller than D131 (56200), D102 (55500), and D149 (66000). The half-width of **11** (78 nm), **12** (100), and **13** (111) were larger than those of D131 (67), D102 (78), and D149 (78), respectively.

2.3. DFT calculations

The structures of **11**, **12**, and **13** were optimized by the B3LYP/3-21G level. The results are shown in Fig. 2 and Table 1. In the case of **11**, the double bond on the 5-position was *E*-form. This comes from less steric repulsion between the hydrogen atom at the 6-position

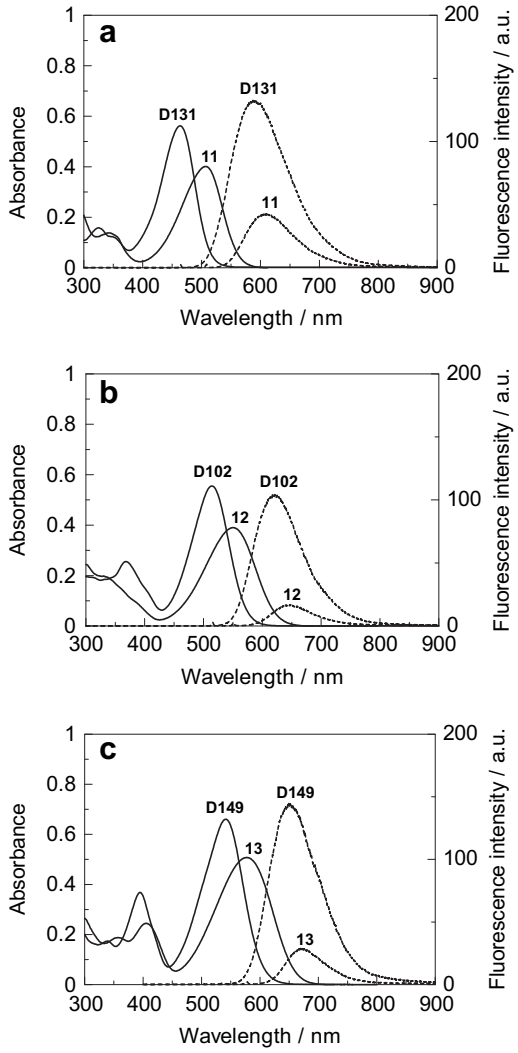

Fig. 1. UV–vis absorption and fluorescence spectra at the concentration of 1.0×10^{-5} mol dm^{-3} in chloroform at 25 °C. (a) **11** and D131, (b) **12** and D102, and (c) **13** and D149. Solid and dotted lines represent UV–vis absorption and fluorescence spectra, respectively.

and methine-hydrogen. Meanwhile, in the case of **12** and **13**, the double bond on the 5-position was *Z*-form. The hydrogen at the 4-position on the benzoindoline moiety and the carbonyl group at the (inner)rhodanine ring was *anti*-form due to steric repulsion between them. The double rhodanine moiety in **13** was *E*-form. The dihedral angles (θ) between the phenylene ring on the nitrogen atom and planar chromophoric moiety of benzoindoline dyes **11** (50.5°), **12** (47.0), and **13** (42.6) were slightly larger than those of indoline dyes D131 (36.0), D102 (37.5), and D149 (37.3), respectively. The dihedral angle of D149 ethyl ester has been reported to be 35° based on single X-ray crystallography [26]. This result comes from steric repulsion between the hydrogen atom at the 2-position on the phenylene ring and that at the 9-position on the benzoindoline moiety. Smaller ϵ values of benzoindoline dyes than the indoline dyes could be attributed to larger dihedral angle.

The HOMO and LUMO energy levels of the optimized structures were calculated by the B3LYP/6-31G(d,p) level. The results are indicated in Fig. 3 and Table 1. The first absorption band of benzoindoline and indoline dyes was attributed to the HOMO–LUMO transition. The significant differences between benzoindoline and indoline dyes were 1) smaller HOMO–LUMO energy gap of benzoindoline derivatives and 2) smaller difference of dipole moment between ground and excited states ($\Delta\mu$) of benzoindoline dyes. Due to the extended conjugation system caused by naphthylene ring, the calculated HOMO energy levels of benzoindoline dyes were higher than those of indoline dyes. No marked effects on LUMO energy level were observed. For example, the HOMO levels of **11** and D131 were calculated to be −5.09 and −5.19 eV, the LUMO levels −2.17 and −2.14 eV, respectively. The $\Delta\mu$ values of **11** and D131 were calculated to be 6.70 and 9.27 debye, respectively. This result may suggest weak electron-injection ability from benzoindoline dyes to zinc oxide compared with that from indoline dyes.

2.4. Photoelectrochemical properties

The UV–vis absorption and IPCE action spectra of benzoindoline and indoline dyes are shown in Fig. 4. The results of photoelectrochemical properties are summarized in Table 2. No clear differences in the UV–vis absorption band of **11** on zinc oxide in the absence and presence of cholic acid (CA) were observed as shown in Fig. 4a. However, the open-circuit photovoltage (V_{oc}) and fill factor (ff) of **11** in the presence of CA were significantly high compared with those in the absence of CA (Table 2, runs 1 and 3). Therefore, the solar-light-to-electricity conversion efficiency (η) in the presence of CA (2.67) was higher than that in the absence of CA (2.15). Thus, the cell performance in the presence of CA was better than that in the absence of CA in all cases (runs 1–12). Fig. 4a also shows that benzoindoline dye **11** is more bathochromic than indoline dye D131 on zinc oxide. Fig. 4b indicates that dye **11** exhibits sensitization at around 550 nm, whereas D131 shows no sensitization at this region. Though the maximum IPCE of **11** (77) was slightly lower than that of

Table 1
Properties of benzoindoline and indoline dyes.

Compd	λ_{max} (ϵ)[a]/nm	F_{max}[a] nm	RFI[b]	SS[c] nm	θ[d] °	HOMO[e] eV	LUMO[e] eV	f[f]	$\Delta\mu$[g] debye
11	343 (13800), 507 (40100)	606	30	99	50.5	−5.09	−2.17	1.23	6.70
D131	325 (15800), 464 (56200)	587	83	123	37.5	−5.19	−2.14	1.40	9.27
12	340 (20500), 551 (39000)	648	12	97	47.0	−5.00	−2.32	1.30	8.33
D102	368 (25600), 514 (55500)	621	68	107	36.0	−5.11	−2.32	1.57	9.74
13	405 (24500), 578 (50800)	670	20	92	42.6	−4.96	−2.39	1.30	8.30
D149	395 (36800), 542 (66000)	649	100	107	37.3	−5.07	−2.37	1.61	9.06

[a] Measured on 1.0×10^{-5} mol dm^{-3} of substrate in chloroform at 25 °C.
[b] Relative fluorescence intensity.
[c] Stokes shift.
[d] Dihedral angle.
[e] Calculated by the B3LYP/6-31G(d,p)/B3LYP/3-21G level.
[f] Oscillator strength calculated by the INDO/S method.
[g] Difference in dipole moment between ground and excited states calculated by the INDO/S method.

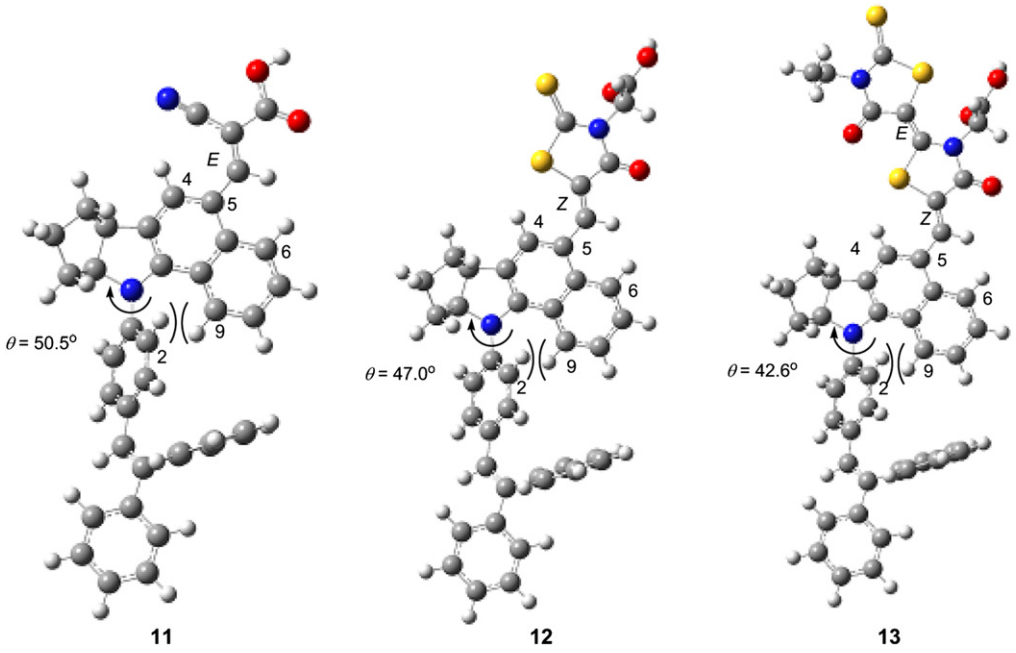

Fig. 2. B3LYP/3-21G optimized structure of **11**, **12**, and **13**.

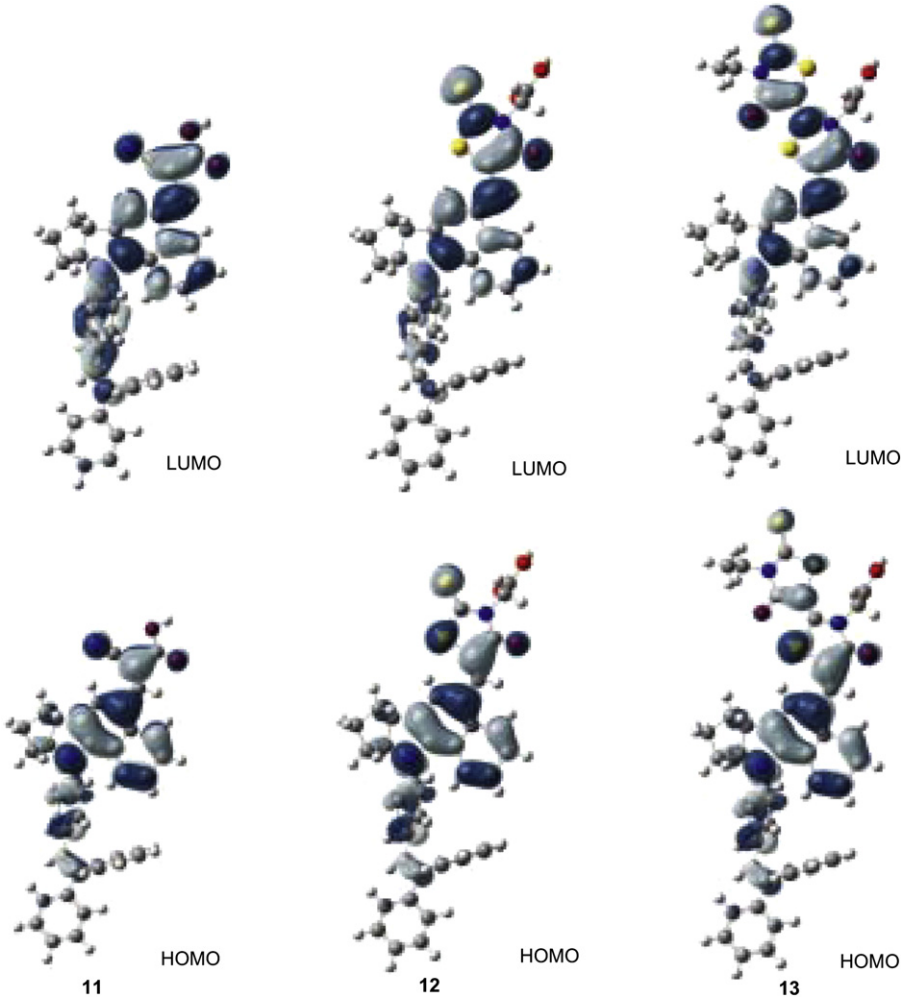

Fig. 3. Calculated HOMO and LUMO electron density in **11**, **12**, and **13**.

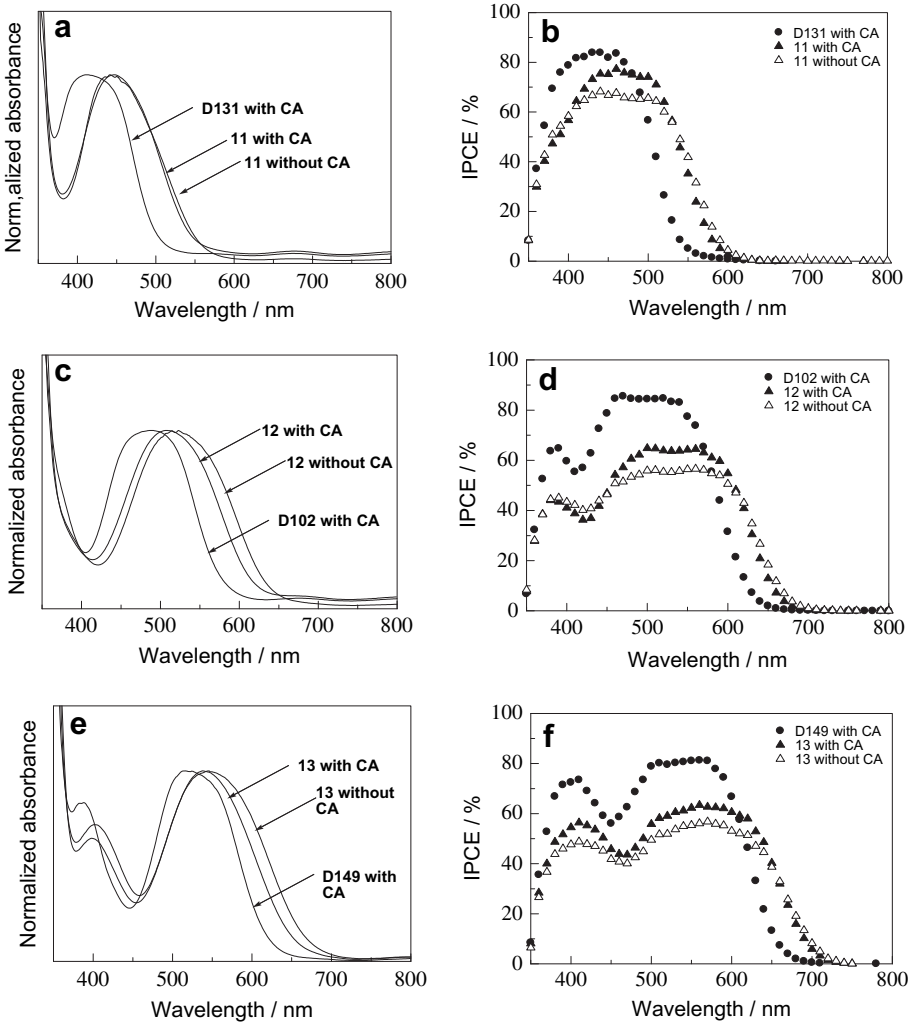

Fig. 4. Normalized UV–vis absorption on zinc oxide and IPCE action spectra. (a) and (b) **11** and D 131, (c) and (d) **12** and D102, (e) and (f) **13** and D149.

D131 (84), the J_{sc} of **11** (6.62) was higher than that of D131 (5.53), due to sensitization at around 550 nm (runs 3 and 4). No remarkable difference in V_{oc} was observed between **11** (0.65) and D131 (0.66) (runs 3 and 4). The ff of **11** (0.62) was lower than that of D131 (0.70) (runs 3 and 4). Consequently, the η value of **11** (2.67) was higher than that of D131 (2.54) (runs 3 and 4).

Table 2
Photoelectrochemical properties of benzoindoline and indoline dyes.

Run	Compd	CA[a]	λ_{max}[b]	Abs[c]	Max IPCE	J_{sc}	V_{oc}	ff	η
			nm		%	mA cm^{-2}	V		%
1	**11**	0	442	3.74	68	6.50	0.58	0.57	2.15
2	D131	0	402	3.79	80	5.70	0.63	0.63	2.27
3	**11**	2	447	1.94	77	6.62	0.65	0.62	2.67
4	D131	2	413	2.37	84	5.53	0.66	0.70	2.54
5	**12**	0	523	3.51	57	8.34	0.48	0.41	1.66
6	D102	0	479	3.81	80	9.65	0.63	0.59	3.55
7	**12**	2	508	1.93	65	8.55	0.58	0.63	3.14
8	D102	2	489	2.23	86	9.12	0.67	0.66	3.99
9	**13**	0	546	3.25	57	8.92	0.57	0.52	2.65
10	D149	0	519	2.99	76	10.81	0.62	0.61	4.11
11	**13**	2	538	2.42	63	9.80	0.62	0.60	3.63
12	D149	2	516	3.36	83	11.67	0.64	0.68	5.06

[a] Molar amount of cholic acid added during dye adsorption process.
[b] Absorption maximum on zinc oxide.
[c] Absorbance on zinc oxide.

Single rhodanine benzoindoline dye **12** showed more bathochromic UV–vis absorption band than D102 on zinc oxide as shown in Fig. 4c. In this case, the absorption band of **12** in the absence of CA was broad compared with that in the presence of CA, indicating aggregates formation. Fig. 4d depicts that the sensitization by **12** occurred at around 630 nm. However, as the maximum IPCE of **12** (65) was smaller than that of D102 (86), the J_{sc} of **12** (8.55) was lower than that of D102 (9.12) (runs 7 and 8). The V_{oc} and ff of **12** (0.58 and 0.63) were lower than those of D102 (0.67 and 0.66) (runs 7 and 8). Therefore, the η of **12** (3.14) was lower than that of D102 (3.99) (runs 7 and 8).

Fig. 4e depicts that the UV–vis absorption band of **13** in the absence of CA was broad compared with that in the presence of CA. Dye **13** showed more bathochromic absorption band than D149. Fig. 4f indicates that dye **13** shows sensitization at around 650 nm. However, as the maximum IPCE of **13** (63) was smaller than that of D149 (83), the J_{sc} of **13** (9.80) was lower than that of D149 (11.67) (runs 11 and 12). The V_{oc} and ff of **13** (0.62 and 0.60) were also lower than those of D149 (0.64 and 0.68) (runs 11 and 12). As the results, the η value of **13** (3.63) was smaller than that of D149 (5.06) (runs 11 and 12).

2.5. Relationship among maximum IPCE, E_{ox}, and E_{ox}–E_{0-0} levels

To understand why only cyanoacrylic benzoindoline dye **11** showed improved cell performance compared with D131, the

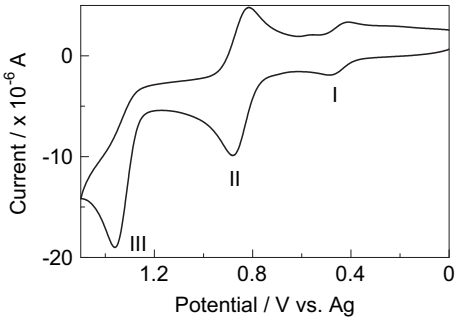

Fig. 5. Electrochemical measurement of **11**. Measured in acetonitrile (2 ml) containing tetrabutylammonium perchlorate (0.1 mol dm^{-3}) and ferrocene (*ca.* 1 mmol dm^{-3}). AgQRE was used as a reference electrode. Platinum wire was used as the working and counter electrodes. The scan rate was 100 mV s^{-1}.

energy diagram was examined. The oxidation potential (E_{ox}) of **11**, **12**, **13**, D131, D102, and D149 was measured in acetonitrile by cyclic voltammetry. Fig. 5 shows the voltammogram of **11** *vs.* Ag *quasi* reference electrode (QRE) in the presence of ferrocene as an internal standard. Three distinct redox waves were observed in the voltammogram. The first oxidative wave (I) at +0.49 V and second wave (II) near +0.88 V *vs.* AgQRE were attributed to the oxidation of ferrocene and **11**, respectively. The third oxidative wave (III) at 1.25 V can come from the further oxidation of **11**. Therefore, the oxidation peak potential (E_{pa}) for **11** is calculated to be +0.39 V *vs.* Fc/Fc$^+$ in acetonitrile. The standard E_{ox} is approximately estimated from the cyclic voltammetric peak potential, which equals to (E_{pa} − 29 mV) if the electrochemical oxidation is a reversible step [27]. Hence, the E_{ox} for **11** was estimated to be +0.36 V *vs.* Fc/Fc$^+$ in this study. The I^-/I_3^- redox level was estimated as −0.05 V *vs.* Fc/Fc$^+$. As no reduction potential peak was observed for benzoindoline and indoline dyes, the potential level of $E_{ox} - E_{0-0}$, corresponding to the reduction potential, was calculated [28]. The λ_{int} which represents the intersection wavelength of normalized UV–vis absorption and the fluorescence spectra of **11** was observed at 554 nm, corresponding to E_{0-0} 2.24 eV. Therefore, the $E_{ox} - E_{0-0}$ value of **11** is calculated to be −1.88 V *vs.* Fc/Fc$^+$. The E_{ox} and $E_{ox} - E_{0-0}$ of the other dyes were obtained in the same way.

As the improved η value of **11** resulted from high J_{sc}, the relationship among maximum IPCE, E_{ox}, and E_{ox}–E_{0-0} levels was examined. The result is shown in Fig. 6. The energy gap between the conduction band of zinc oxide (−0.95 V) and E_{ox}–E_{0-0} level of dyes is 0.72–0.99 V. Meanwhile, that between I^-/I_3^- redox potential and E_{ox} levels is 0.34–0.52 V. Though the maximum IPCE of D149 (83%) is higher than that of **12** (63%), the E_{ox}-E_{0-0} level of D149 (−1.70 V) is less negative than that of **12** (−1.76 V). It is reported that the maximum IPCE of *N*-(4-substituted phenyl) double rhodanine indoline dyes decreases by introducing electron-donating substituent such as diphenylamino and dimethylamino groups [28]. In the case of titanium oxide, the energy gap of 0.2–0.3 V is required to proceed the electron transfer [29,30]. Therefore, the E_{ox} level of indoline dyes is more important than the $E_{ox} - E_{0-0}$ level to control the maximum IPCE. It is clear that the E_{ox} level of benzoindoline dyes **11** (+0.36), **12** (+0.29), and **13** (+0.26) is less positive than the respective indoline dyes D131 (+0.47), D102 (+0.40), and D149 (+0.40), due to electron-rich benzoindoline skeleton. Among the benzoindoline dyes, the cyanoacrylic derivative **11** (+0.36) showed the most positive E_{ox} level followed by single **12** (+0.29) and double rhodanine derivatives **13** (+0.26). Therefore, only cyanoacrylic benzoindoline dye **11** having sufficiently positive E_{ox} level and bathochromic UV–vis absorption band could show larger J_{sc} than D131 to improve η. To improve the cell performance of single and double rhodanine benzoindoline dyes, it is important to introduce electron-withdrawing moiety(ies) into the molecules to cause positive shift of the E_{ox} level.

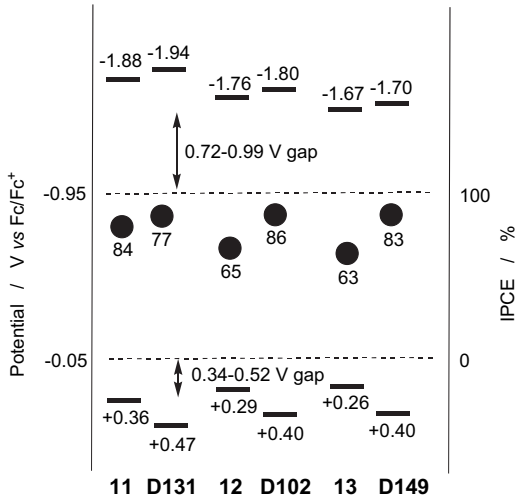

Fig. 6. Relationship among IPCE, E_{ox}, and E_{ox}–E_{0-0x} levels of benzoindoline and indoline dyes.

3. Conclusion

The cell performance of three series of novel benzoindoline dyes was compared with that of known indoline dyes. Only cyanoacrylic benzoindoline dye showed improved cell performance due to larger J_{sc} value. This could result from its positive E_{ox} level and bathochromic UV–vis absorption band.

4. Experimental

4.1. Instruments

Melting points were measured with a Yanaco MP-13 micro-melting-point apparatus. NMR spectra were taken with a JEOL JNM-ECX 400P spectrometer. Mass spectra were taken on JEOL MStation 700 and JMS-AMSUN200/GI GCMS spectrometers. UV–vis absorption and fluorescence spectra were taken on Hitachi U-3500 and F-4500 spectrophotometers, respectively.

4.2. Materials

2-Cyclopentanone (**2**), cyanoacrylic acid (**8**), and rhodanine acetic acid (**9**) were purchased from Tokyo Kasei Co., Ltd. 1-Bromo-4-(2,2-diphenylethenyl)benzene (**5**), double rhodanine acetic acid **10**, D131, D102, and D149 were supplied from Chemicrea Co., Ltd. 1-Naphthylhydrazine hydrochloric acid salt was synthesized as describe in the literature [31].

4.3. Synthesis of 7,8,9,10-tetrahydrobenzo[g]cyclopenta[b]indole (*3*)

1-Naphthylhydrazine hydrochloric acid salt (607 mg, 3.13 mmol) was dissolved in aqueous sodium acetate. The free base was extracted with dichloromethane. To this free base was added an acetic acid solution (3 ml) of cyclopentanone (269 mg, 3.20 mmol). The mixture was refluxed for 2 h. The hot reaction mixture was poured onto ice. The resulting precipitate was filtered and purified by silica gel column chromatography (CH_2Cl_2:C_6H_{14} = 5:1). Yield 55%; mp 167–170 °C; ^{1}H NMR ($CDCl_3$)

δ = 2.58 (quin, J = 6.9 Hz, 2H), 2.90 (t, J = 6.9 Hz, 2H), 2.95 (t, J = 6.9 Hz, 2H), 7.36 (t, J = 8.3 Hz, 1H), 7.47 (t, J = 8.3 Hz, 1H), 7.48 (d, J = 8.7 Hz, 1H), 7.57 (d, J = 8.7 Hz, 1H), 7.89 (d, J = 8.3 Hz, 1H), 7.92 (d, J = 8.3 Hz, 1H); EIMS (70 eV) m/z (rel intensity) 207 (M^+, 100), 180 (31), 103 (20).

4.4. Synthesis of 6b,7,8,9,9a,10-hexahydrobenzo[g]cyclopenta[b] indole (**4**)

To an acetic acid suspension (5 ml) of 7,8,9,10-tetrahydrobenzo [*g*]cyclopenta[*b*]indole **3** (212 mg, 1.02 mmol) was added sodium borohydride (80 mg, 2.12 mmol) below 35 °C. The mixture was stirred one day at room temperature. After the reaction was completed, water was added. The product was extracted with dichloromethane and purified by silica gel column chromatography (CH_2Cl_2:C_6H_{14} = 5:1). Yield 68%; oil; ^{1}H NMR ($CDCl_3$) δ = 1.26–1.38 (m, 1H), 1.56–1.59 (m, 1H), 1.67–1.77 (m, 3H), 1.86–1.95 (m, 1H), 3.83–3.87 (m, 1H), 4.42–4.44 (m, 1H), 6.21 (br s, 1H), 7.02 (d, J = 7.8 Hz, 1H), 7.14 (d, J = 7.8 Hz, 1H), 7.24–7.30 (m, 2H), 7.65–7.68 (m, 1H), 7.71–7.73 (m, 1H); EIMS (70 eV) m/z (rel intensity) 209 (M^+, 45), 180 (100).

4.5. Synthesis of 10-[4-(2,2-diphenylethenyl)phenyl]-6b,-7,8,9,9a,10-hexahydrobenzo[g]cyclopenta[b]- indole (**6**)

To xylene solution (10 ml) of 6*b*,7,8,9,9*a*,10-tetrahydrobenzo[*g*] cyclopenta[*b*]indole (731 mg, 2.32 mmol) were added 1-bromo-4-(2,2-diphenylethenyl)benzene (**5**) (476 mg, 2.27 mmol), potassium *tert*.-butoxide (310 mg, 2.76 mmol), palladium acetate (10 mg, 0.05 mmol), and tri-*t*-butylphosphine (13 mg, 0.06 mmol). The mixture was heated at 120 °C for 16 h. After the reaction was completed, the product was filtered using celite. The product was washed with 2 N hydrochloric acid and purified by silica gel column chromatography (CH_2Cl_2 : C_6H_{14} = 2:1). Yield 69%; mp 79–82 °C; ^{1}H NMR ($CDCl_3$) δ = 1.17–1.26 (m, 1H), 1.49–1.56 (m, 1H), 1.72–1.75, (m, 1H), 1.80–1.87 (m, 1H), 1.96–2.05 (m, 2H), 4.08–4.11 (m, 1H), 4.29–4.32 (m, 1H), 6.64 (d, J = 8.7 Hz, 2H), 6.85 (d, J = 8.7 Hz, 2H), 7.01 (s, 2H), 7.07–7.41 (m, 14H), 7.47 (d, J = 8.2 Hz, 1H), 7.81 (d, J = 8.2 Hz, 1H); EIMS (70 eV) m/z (rel intensity) 463 (M^+, 100), 434 (23).

4.6. Synthesis of 10-[4-(2,2-diphenylethenyl)phenyl]-6b,7,8,9,9a,10-hexahydrobenzo[g]- cyclopenta[b]indole-5-carbaldehyde

To DMF (1 ml) was added phosphoryl chloride (252 mg, 1.64 mmol) at 10 °C. The mixture was stirred for 30 min. To this mixture was added a DMF solution of 10-[4-(2,2-diphenylethenyl)phenyl]-6*b*,7,8,9,9*a*,10-hexahydrobenzo[*g*]cyclopenta[*b*]indole **6**(327 mg, 0.71 mmol) below 20 °C. The mixture was stirred for 2 h. After the reaction was completed, the mixture was poured onto ice and neutralized with aqueous sodium hydroxide. The product was extracted with dichloromethane and purified by silica gel column chromatography (CH_2Cl_2). Yield 63%; mp 193–195 °C; ^{1}H NMR ($CDCl_3$) δ = 1.26–1.32 (m, 1H), 1.57–1.59 (m, 1H), 1.82–1.88, (m, 3H), 2.01–2.08 (m, 1H), 4.07–4.11 (m, 1H), 4.57–4.62 (m, 1H), 6.91 (d, J = 8.2 Hz, 2H), 6.98 (d, J = 8.2 Hz, 2H), 7.09 (s, 1H), 7.15–7.42 (m, 12H), 7.51 (t, J = 8.3 Hz, 1H), 7.92 (s, 1H), 9.19 (d, J = 8.3 Hz, 1H), 10.05 (s, 1H); EIMS (70 eV) m/z (rel intensity) 491 (M^+, 100), 462 (16).

4.7. Synthesis of **11**

To acetonitrile (5 ml) were added **7** (254 mg, 0.52 mmol), cyanoacetic acid **8** (121 mg, 1.42 mmol), and piperidine (57 mg, 0.67 mmol). The mixture was refluxed for 120 °C. Then, to the mixture was added chloroform and 2 N aqueous hydrochloric acid. The organic layer was separated, washed with water, and dried over anhydrous sodium sulfate. The product was isolated by column chromatography (SiO_2, $CHCl_3$). Yield 53%; mp 135–138 °C; ^{1}H NMR ($CDCl_3$) δ = 1.26–1.32 (m, 1H), 1.56–1.58 (m, 1H), 1.79–1.86 (m, 3H), 2.01–2.07 (m, 1H), 4.07–4.10 (m, 1H), 4.62–4.65 (m, 1H), 6.93 (d, J = 7.6 Hz, 2H), 6.98 (d, J = 7.6 Hz, 2H), 7.10 (s, 1H), 7.15–7.16 (m, 3H), 7.21–7.35 (m, 7H), 7.40 (t, J = 7.6 Hz, 2H), 7.50 (t, J = 7.6 Hz, 1H), 8.06 (d, J = 8.9 Hz, 1H), 8.38 (s, 1H), 8.85 (s, 1H); FABHRMS m/z 559.2390 (MH^+), calcd for $C_{39}H_{31}N_2O_2$ 559.2386.

4.8. Synthesis of **12**

To acetic acid (8 ml) were added **7** (254 mg, 0.52 mmol) and **8** (103 mg, 0.54 mmol). The mixture was heated to 120 °C. Then, to the mixture was added ammonium acetate (18 mg, 0.23 mmol). The mixture was heated at 120 °C for 90 min. After the reaction was completed, to the mixture was added water. The resulting precipitate was filtered and washed with water and methanol. The product was isolated by column chromatography (SiO_2, $CHCl_3$). Yield 34%; mp 159–162 °C; ^{1}H NMR ($CDCl_3$) δ = 1.30–1.34 (m, 1H), 1.56–1.61 (m, 1H), 1.80–1.89 (m, 3H), 2.04–2.11 (m, 1H), 4.12–4.14 (m, 1H), 4.58–4.61 (m, 1H), 6.89 (d, J = 7.9 Hz, 2H), 6.97 (d, J = 7.6 Hz, 2H), 7.08 (s, 1H), 7.15–7.19 (m, 3H), 7.24–7.41 (m, 9H), 7.52 (t, J = 7.9 Hz, 1H), 7.58 (s, 1H), 8.18 (d, J = 8.2 Hz, 1H), 8.44 (s, 1H); FABHRMS m/z 665.1917 (MH^+), calcd for $C_{41}H_{33}N_2O_3S_2$ 665.1933.

4.9. Synthesis of **13**

To acetic acid (8 ml) were added **7** (0.230 g, 0.47 mmol) and **9** (0.151 g, 0.47 mmol). The mixture was heated to 120 °C. Then, to the mixture was added ammonium acetate (0.021 g, 0.27 mmol). The mixture was heated at 120 °C for 90 min. After the reaction was completed, to the mixture was added water. The resulting precipitate was filtered and washed with water and methanol. The product was isolated by column chromatography (SiO_2, $CHCl_3$). Yield 28%; mp 226–228 °C; ^{1}H NMR ($CDCl_3$) δ = 1.14 (t, J = 6.8 Hz, 3H), 1.30–1.33 (m, 1H), 1.60–1.62 (m, 1H), 1.85–1.91 (m, 3H), 2.05–2.17 (m, 1H), 4.02 (q, J = 6.8 Hz, 2H), 4.15–4.19 (m, 1H), 4.56–4.61 (m, 1H), 4.81 (s, 2H), 6.87 (d, J = 8.0 Hz, 2H), 6.96 (d, J = 8.0 Hz, 2H), 7.08 (s, 1H), 7.15–7.42 (m, 12H), 7.50 (t, J = 7.3 Hz, 1H), 7.69 (s, 1H), 8.15 (d, J = 8.7 Hz, 1H), 8.44 (s, 1H); FABHRMS m/z 792.1974 (MH^+), calcd for $C_{46}H_{38}N_3O_4S_3$ 792.2024.

4.10. Preparation of zinc oxide solar cell

An aqueous potassium chloride solution (300 ml, 0.1 mol dm^{-3}) was electrolyzed at −1.0 V *vs.* SCE with bubbling an oxygen gas at 70 °C for 30 min. Platinum was used as a counter electrode. To the pre-electrolyzed film was added an aqueous solution of zinc chloride (5 mmol dm^{-3}). Then, the film was electro-deposited again in the solution at −1.0 V vs. SCE at 70 °C for 20 min with bubbling an oxygen gas. To the electro-deposited film was added an aqueous solution of Eosin Y (50 μmol dm^{-3}). The film was electro-deposited at −1.0 V vs. SCE at 70 °C for 30 min with bubbling an oxygen gas. The film was kept in a diluted aqueous potassium hydroxide solution (pH 10.5) for 24 h to remove adsorbed Eosin Y. The film was dried at 100 °C for 1 h. The thin film was immersed in a chloroform solution of dye (1×10^{-4} mol dm^{-3}) and kept at ambient temperature for 1 h to adsorb dyes **11**, **12**, and **13**. In the cases of D131, D102, and D149, the film was immersed in an acetonitrile-*tert*.-butyl alcohol 1:1 mixed solution (5×10^{-4} mol dm^{-3}). Then, the film was washed with chloroform. The films were dried under an air atmosphere at ambient temperature. The film was used as the working electrode. Platinum spattered film was used as a counter

electrode. The cell size was 5.0 mm × 5.0 mm. Thermosetting resin was put around the cell. An acetonitrile–ethylenecarbonate ($v/v = 1/4$) mixed solution containing tetrabutylammonium iodide (0.5 mol dm^{-3}) and iodine (0.05 mol dm^{-3}) was used as an electrolyte.

4.11. Photoelectrochemical measurements

An action spectrum was measured under monochromatic light with a constant photon number (5×10^{15} photon cm^{-2} s^{-1}). *I–V* characteristics were measured under illumination with AM 1.5 simulated sunlight (100 mW cm^{-2}) through a shading mask (5.0 mm × 4.0 mm).

4.12. Electrochemical measurements

Electrochemical measurement was performed in acetonitrile. The oxidation potential was measured by using small-size three electrodes. Ag *quasi* reference electrode (QRE) was used as a reference. Platinum wire was used as the working and counter electrodes. All electrode potentials were calibrated with respect to ferrocene (Fc)/ferrocenium (Fc^+) redox couple. An acetonitrile solution (2 ml) of dyes containing tetrabutylammonium perchlorate (0.1 mol dm^{-3}) and ferrocene (*ca.* 1 mmol dm^{-3}) was prepared. The electrochemical measurement was performed at the scan rate of 100 mV s^{-1}.

Acknowledgement

This work was financially supported in part by Grants-in-Aid for Science Research (No. 21550180) from Japan Society for the Promotion of Science (JSPS) and Research for Promoting Technological Seeds.

References

[1] Zhang G, Bala H, Cheng Y, Shi D, Lv X, Yu Q, et al. High efficiency and stable dye-sensitized solar cells with an organic chromophore featuring a binary π-conjugated spacer. Chem Commun; 2009:2198–200.
[2] Ning Z, Tian H. Triarylamine, a promising core unit for efficient photovoltaic materials. Chem Commun; 2009:5483–95. and references cited therein.
[3] Kim S, Kim D, Choi H, Kang M-S, Song K, Kang O-S, et al. Enhanced photovoltaic performance and long-term stability of quasi-solid-state dye-sensitized solar cell via molecular engineering. Chem Commun; 2008:4951–3.
[4] Wang Z-S, Koumura N, Cui Y, Takahashi M, Sekiguchi H, Mori A, et al. Hexylthiophene-functionalized carbazole dyes for efficient molecular photovoltaics: tuning of solar-cell performance by structural modification. Chem Mater 2008;20:3993–4003.
[5] Kuang D, Uchida S, Humphry-Baker R, Zakeeruddin SM, Grätzel M. Organic dye-sensitized ionic liquid based solar cells: remarkable enhancement in performance through molecular design of indoline sensitizers. Angew Chem Int Ed 2008;47:1923–7.
[6] Schmidt-Mende L, Bach U, Humphry-Baker R, Horiuchi T, Miura H, Ito S, et al. Organic dye for highly efficient solid-state dye-sensitized solar cells. Adv Mater 2005;17:813–5.
[7] Horiuchi T, Miura H, Uchida S. Highly efficient metal-free organic dyes for dye-sensitized solar cells. J Photochem Photobiol A Chemistry 2004;164:29–32.
[8] Horiuchi T, Miura H, Sumioka K, Uchida S. High efficiency of dye-sensitized solar cells based on metal-free indoline dyes. J Am Chem Soc 2004;126:12218–9.
[9] Horiuchi T, Miura H, Uchida S. Highly-efficient metal-free organic dyes for dye-sensitized solar cells. Chem Commun; 2003:3036–7.
[10] Ito S, Zakeeruddin SM, Humphry-Baker R, Liska P, Charvet R, Comte P, et al. High-efficiency organic-dye-sensitized solar cells controlled by nanocrystalline-TiO_2 electrode thickness. Adv Mater 2006;18:1202–5.
[11] Ito S, Miura H, Uchida S, Takata M, Sumioka K, Liska P, et al. High-conversion-efficiency organic dye-sensitized solar cells with a novel indoline dye. Chem Commun; 2008:5194–6.
[12] Dentani T, Kubota Y, Funabiki K, Jin J, Yoshida T, Minoura H, et al. Novel thiophene-conjugated indoline dyes for zinc oxide solar cells. New J Chem 2009;33:93–101.
[13] Matsui M, Ito A, Kotani M, Kubota Y, Funabiki K, Jin J, et al. The use of indoline dyes in a zinc oxide dye-sensitized solar cell. Dyes Pigments 2009;80:233–8.
[14] Jose R, Kumar A, Thavasi V, Fujihara K, Uchida S, Ramakrishna S. Relationship between the molecular orbital structure of the dyes and photocurrent density in the dye-sensitized solar cells. Appl Phys Lett 2008;93:023125/1–023125/3.
[15] Tanaka H, Takeichi A, Higuchi K, Motohiro T, Takata M, Hirota N, et al. Long-term durability and degradation mechanism of dye-sensitized solar cells sensitized with indoline dyes. Sol Energy Mater Sol Cells 2009;93:1143–8.
[16] Li XD, Zhang DW, Sun Z, Chen YW, Huang SM. Metal-free indoline-dye-sensitized TiO_2 nanotube solar cells. Microelectr J 2009;40:108–14.
[17] Kuang D, Brillet J, Chen P, Takata M, Uchida S, Miura H, et al. Application of highly ordered TiO_2 nanotube arrays in flexible dye-sensitized solar cells. ACS Nano 2008;2:1113–6.
[18] Wijayarathna TRCK, Aponsu GMLP, Ariyasinghe YPYP, Premalal EVA, Kumara GKR, Tennakone K. A high efficiency indoline-sensitized solar cell based on a nanocrystalline TiO_2 surface doped with copper. Nanotechnology 2008;19:485703/1–485703/5.
[19] Jose R, Kumar A, Thavasi V, Ramakrishna S. Conversion efficiency versus sensitizer for electrospun TiO_2 nanorod electrodes in dye-sensitized solar cells. Nanotechnology 2008;19:424004/1–424004/7.
[20] Yoshida T, Zhang J, Komatsu D, Sawatani S, Minoura H, Pauporté T, et al. Electrodeposition of inorganic/organic hybrid thin films. Adv Func Mater 2009;19:17–43.
[21] Yoshida T, Hiramatsu K, Koike H, Yane T, Funabiki K, Matsui M, et al. Colorful and plastic solar cells with electrodeposited nanostructured zinc oxide. Galvanotechnik 2009;100:164–8.
[22] Howie WH, Claeyssens F, Miura H, Peter LM. Characterization of solid-state dye-sensitized solar cells utilizing high absorption coefficient metal-free organic dyes. J Am Chem Soc 2008;130:1367–75.
[23] Konno A, Kumara GRA, Kaneko S, Onwona-Agyeman B, Tennakone K. Solid-state solar cells sensitized with indoline dye. Chem Lett 2007;36:716–7.
[24] Miyoshi K, Numao M, Ikegami M, Miyasaka T. Effect of thin TiO_2 buffer layer on the performance of plastic-based dye-sensitized solar cells using indoline dye. Electrochemistry 2008;76:158–60.
[25] Ogura RY, Nakane S, Morooka M, Orihashi M, Suzuki Y, Noda K. High-performance dye-sensitized solar cell with a multiple dye system. Appl Phys Lett 2009;94:073308/1–073308/3.
[26] Matsui M, Fujita T, Kubota Y, Funabiki K, Miura H, Shiro M. X-ray crystallography of D149 ethyl ester. Bull Chem Soc Jpn 2010;83:709–11.
[27] Nicholson RS, Shain I. Theory of stationary electrode polarography. Single scan and cyclic methods applied to reversible, irreversible, and kinetic systems. Anal Chem 1964;36:706–23.
[28] Matsui M, Fujita T, Kubota Y, Funabiki K, Jin J, Yoshida T, et al. Substituent effect in double rhodanine indoline dye on performance of zinc oxide dye-sensitized solar cell. Dye Pigments 2010;86:143–8.
[29] Hara K, Sato T, Katoh R, Furube A, Ohga Y, Shinpo A, et al. Molecular design of coumarin dyes for efficient dye-sensitized solar cells. J Phys Chem B 2003;107:597–606.
[30] Hara K, Sato T, Katoh R, Furube A, Yoshihara T, Murai M, et al. Novel conjugated organic dyes for efficient dye-sensitized solar cells. Adv Funct Mater 2005;15:246–52.
[31] Portoghese PS, Sultana M, Takemori AE. Design of peptidomimetic δ opioid recepter antagonists using the message-address concept. J Med Chem 1990;33:1714–20.